
Article:
Brif, A., Laity, P., Claeyssens, F. orcid.org/0000-0002-1030-939X et al. (1 more author) (2020) Dynamic photo-cross-linking of native silk enables macroscale patterning at a microscale resolution. ACS Biomaterials Science & Engineering, 6 (1). pp. 705-714. ISSN 2373-9878

https://doi.org/10.1021/acsbiomaterials.9b00993

Dynamic Photo-crosslinking of Native Silk Enables Macro-scale Patterning at Micro-scale Resolution

Anastasia Brif [1,2], Peter Laity [1], Frederik Claeyssens [2] and Chris Holland* [1]*

[1]Department of Materials Science and Engineering Sir Robert Hadfield Building, Mappin Street, University of Sheffield, Sheffield, S1 3JD, UK

[2]Department of Materials Science and Engineering, Kroto Research Institute, Broad Lane, University of Sheffield, Sheffield S3 7HQ, UK

Corresponding Authors

1. Chris Holland*

   Email: christopher.holland@sheffield.ac.uk

   Telephone**:** +44 (0) 114 222 5477

2. Frederik Claeyssens*

   Email: f.claeyssens@sheffield.ac.uk

   Telephone**:** +44 (0) 114 222 5513

KEYWORDS: Silk, riboflavin, light, mask-less lithography, micro-patterning, rheology

ABSTRACT

Light-based structuring methods have shown reconstituted silk to be a versatile and appropriate material for a range of optical and biomaterial-based applications. However, without an understanding of how an unmodified, native, silk responds to photo-processing, the full potential of this material cannot be realized. Here, we show that the use of native silk enables the production of compound patterns with improved resolution and image quality when quantitatively compared to standard reconstituted silk, which we link directly to the influence of molecular weight. Further insights into the mechanism behind silk structure development are provided through mechanical (rheological) and structural (FTIR) measurements and results show that processing can tune properties over several orders of magnitude, enabling potential replication of several soft tissue types. Finally, broadening our application perspective, this combination of mask-less lithography and native silk resulted in the fabrication of transparent optical elements for data storage and labeling.

INTRODUCTION

Silk fibers have been used for centuries in both textile and medical applications[1–3]. Today, silk is finding utility in a wide range of devices, as it can be readily resolubilised and formed into a plethora of different structures[4–6]. This makes silk compatible for applications in diverse research areas such as tissue engineering[7,8], drug delivery[9], optics[10,11], electronics[12] and surface engineering[13–15]. Yet despite this impressive range of applications, manufacturing processes are still largely focused on bulk random structuring in order to achieve functionality.

Fortunately, the past decade has seen a rapid increase in techniques to facilitate precision control of silk structures at the micro and nanoscale, particularly in the area of bio-optics[16,17]. These approaches can be divided into indirect and direct routes. Indirect fabrication routes such as soft lithography[18,19], nano-imprinting[20], and classical photo-lithography[21–23], whilst inexpensive, require pre-fabrication of fixed templates, masks, and molds to form the final patterns which can often constrain the resulting structure and its resolution. Direct routes, including e-beam[11,24], laser machining[25] and multi-photon lithography[26,27], allow one to achieve much higher pattern resolution; however, these methods usually involve high-cost equipment, small patterning areas, prior chemical modification and require longer fabrication times[16,28].

To address such challenges, we present projection micro-stereolithography (PμSL)[29–32] as a new route for high resolution silk patterning. PμSL is a 3D printing technique based on photocuring a (bio)polymer solution[33–35]. Importantly it utilizes a digital micro-mirror device (DMD)[32,36] as a dynamic mask, thus replacing the need of a pre-fabricated static photomask[37]. Furthermore a dynamic mask such as this enables much greater control over shape and mechanical properties of the projected pattern on a sub-micron resolution and does not require the fabrication of a single-purpose mask or the time constraints of single pixel fabrication[38,39].

Creation of a silk based solution prior to patterning is traditionally achieved through reconstitution; a process where spun silk is exposed to chaotropic agents to enable resolubilisation[40]. Unfortunately, if reconstitution is not carefully controlled, it can result in a certain degree of collateral damage to the fibroin and may lead to a decrease in the molecular weight of the protein, which also impacts the properties of the final restructured material[41,42]. In fact, we posit that reconstitution's degrading effect on the silk protein may explain why current silk photo-curing techniques require relatively high silk concentrations (>5 wt%) in order to generate stable structures[22,27,43].

Alternatively, it is possible to obtain a soluble, native, silk solution directly extracted from the animal's silk gland[44–46]. The use of such native silk solutions has previously been shown to be advantageous not only in setting the gold standard for biomimetic spinning technologies[45,47–50] and even perhaps as a model biopolymer[51,52] but also recently in creating silk based encapsulation devices[53] and in the development of silk based biophotonics[17] at relatively low silk concentrations (~1 wt%). However, the potential of native silks for deployment in photolithographic applications have yet to be fully exploited, and hence the impetus for this work.

In this paper, we present a direct, water-based route, for micro silk patterning using photo-curable *Bombyx mori* native silk feedstock solution and PμSL without prior chemical modification. The method not only allows control over the pattern on a micron resolution level but also produces large-scale (1 cm^2) repetitive patterns. In addition, we show the influence of molecular weight in this structuring approach by comparing native silk feedstock, reconstituted silk protein and a tyrosine-rich synthetic protein solution to validate the structuring mechanism.

EXPERIMENTAL METHODS

Protein solution fabrication: Native silk feedstock was extracted from the sericin-free section of the dope[48,54,55], which is the posterior section of the middle division from final instar *B. mori* silkworms and diluted in Type II water so that the protein concentration was 1 wt%. No further purification was required. Reconstituted silk (RS) solution was prepared in accordance with the protocol described elsewhere[6]. In short, silk cocoons where cut into small pieces and degummed in Na_2CO_3 for 30 minutes. The degummed silk was dried and then dissolved in 9.3 M LiBr solution at 60°C for 1 h. The ratio between silk and LiBr solution was 1:10. After full dissolution, the solution was transferred into a dialysis membrane (MWCO 12-14 kD, Spectra/por®) and placed in DI water to remove the remaining LiBr. The water was changed 10 times over 24 h. The resulting RS solution was diluted to 2 wt%. Poly(Glu-co-Tyr) (Sigma-Aldrich) was diluted in Type II water to 5 wt%. After preparation, all solutions were stored at 4°C and were used within 1 week to avoid any age-related degradation of the polymers.

Photo-curable solution fabrication: Photo-curable protein solution was produced by the addition of 0.02 wt% of riboflavin 5′-monophosphate (Sigma-Aldrich). All solutions were kept in the dark prior to use to avoid initiation of the crosslinking reaction.

Silk patterning: The patterns were fabricated by projection-based lithography using a digital micro-mirror device (DMD). Light from a violet diode laser (405 nm, Vortran laser technology Inc, Sacramento, CA, USA) was expanded to a 5 mm diameter beam and was reflected from a DLP® 0.55 XGA DMD with 5.4 μm mirror size (Texas Instruments Incorporated, TX, USA). The reflected image was directed by a silver coated mirror and projected onto a glass slide covered with photo-curable protein solution, located below the mirror. The solution was confined in a frame to ensure a flat surface area and covered during the photo-curing process to avoid water

evaporation. The laser power was 250 mW and projection time varied from 10 s to 10 min for all types of samples.

Post-fabrication treatment: After fabrication, dry samples were immersed in 9.3 M LiBr solution for 10 min at 60°C and then in DI water for 10 min at room temperature. This eluted non-structured protein solution prior to any mechanical analysis. To induce silk crystallization, the patterns were immersed for 1 min in MeOH/DI solution at concentration range from 10 to 100 (v/v %). The samples left to dry and rehydrated with DI water prior to any measurements.

Imaging: Optical images of the structures were collected by Diaphot TMD300 microscope (Nikon Instruments, Japan) using a Moticam 5MP camera (Motic instruments, Spain) and Stemi 305 microscope (Zeiss, Germany) using an Axiocam 105 color camera (Zeiss, Switzerland). Optical profilometry images were collected by ContourGT-X 3D (Bruker, USA). All images were analyzed by ImageJ (1.48v).

Characterization of the crosslinked patterns: All spectral data was acquired at room temperature (25±2°C). Samples were characterized by Fourier-transform infrared spectroscopy (FTIR) using a Nicolet 380 spectrometer (Thermo Scientific, Madison, USA) equipped with a Golden Gate attenuated total reflection (ATR) device (Specac, UK). Spectral data were collected between 800 and 4000 cm^{-1}, using 64 scans, at 4 cm^{-1} resolution. UV-VIS absorption spectra were collected (using Spectronic Unicam, UV 330, UK), in the spectral range between 230 nm and 600 nm. Peaks in the spectra were fitted using MagicPlot Student Version 2.7.2. All peaks were fitted as Gaussians.

Similarity analysis of the patterns: A similarity index was defined to evaluate how similar the fabricated patterns were to the original projected pattern. To achieve this, a photo of each pattern was collected by an optical microscope. Then the image was transferred to ImageJ software for

further analysis. For each image (original projected image and the resulted pattern), a threshold was adjusted to 70 % and a binary function was applied. Then any noise or contamination in the image, outside of the pattern, was removed by coloring the relevant pixel in black, assuring that no pixel from the pattern was removed. The fabricated pattern was tinted in grey to introduce color contrast. Then the binary images of the fabricated pattern (grey) and the original image (white) were overlaid to evaluate the correlation between the images (see Figure 3S in supplementary data). The histogram of the overlay image was plotted, containing 4 peaks corresponding to pixel counts of the following regions on the image: Black - background (no pixels in original and fabricated images); Dark grey- no correlation (pixel present in fabricated pattern but not in the original image); Light grey – correlation (pixel present in both images); White - original pattern (pixel present in original image but not in the fabricated pattern). The similarity percent was defined as the number of correlating pixels between the original image and the received pattern divided by the original image. For each sample type, at least 3 images were analyzed, and similarity values were averaged.

QR code, image analysis: Optical images of the QR code pattern were collected by Diaphot TMD300 microscope (Nikon Instruments, Japan) and analyzed by ImageJ (1.48v). Minimal image processing was applied, to enhance the contrast between the pattern and the background (binary→ invert→ erode). The codes were scanned by a QR Scanner app (version 0.52) installed on a mobile phone (Sony Xperia Z3 compact).

Rheological measurements: A sample's elastic modulus (G′) was recorded using AR 2000 and Discovery HR-2 rheometers (TA Instruments, New Castle, DE, USA). The latter was equipped with the modular microscope accessory, with a transparent lower plate and a 405 nm LED light source (minimum power output 870 mW), to enable *in situ* photo-curing experiments. The

geometry for all measurements was an 8 mm parallel plate. All rheological data was acquired at room temperature (25 ± 2°C). To avoid water evaporation, wet tissue was placed around the sample and the sample was covered with a customized environmental chamber which was not in contact with the geometry of the rheometer at any time. The experiments were performed in two stages, an oscillatory frequency sweep (20 to 0.1 Hz) followed by a fixed frequency time ramp (1 Hz), both of which were conducted within the sample's linear viscoelastic region (target strain 0.01). For the oscillatory test, presented modulus values were calculated as the average G' value in the range between 1 to 10 Hz. The 405 nm LED light source was turned on and off during the experiment at given intervals to explore the change in elastic modulus upon irradiation.

Protein analysis by gel electrophoresis: A small portion of each solution (1 wt%) was mixed with an equal volume of a solution containing sodium dodecyl sulfate (SDS, 4 %, to disrupt non-covalent bonding) and 2-mercaptoethanol (4 mM, to reductively cleave disulfide bonds in the proteins). 20 µL of each solution was loaded onto on a 4–20 % polyacrylamide (PA) gradient gel and the protein components were separated by electrophoresis (GE) (90 minutes, 160 V, 100 mA). The gel was immersed for 30 minutes into a fixation solution (400 mL ethanol, ethanoic 100 mL acid, 500 mL water) and protein bands were stained by Coomassie blue. The gel was imaged using a Perfection 2450 Photo scanner (Seiko Epson Corp. Suwa, Japan) at 1200 DPI. Molecular weights of the proteins were evaluated by comparing their movement with reference standards (HiMark™ Pre-stained High Molecular Weight Protein Standard).

RESULTS AND DISCUSSION

When dealing with native silk proteins, it is important to keep in mind the high sensitivity of these materials to their environmental conditions. Various parameters such as temperature change[56], variations in pH[57–59], mechanical shear[48,50,60,61], the presence of solvents[62] and time[63],

are known to induce gelation/solidification in silk protein solutions. Therefore, in order to achieve control over our fabrication process we opted to keep this process as simple as possible, introducing the minimum amount of chemical reagents into the silk solution.

In this work, photo-curable native silk was obtained solely by the addition of a water-soluble formulation of riboflavin to act as a photo-initiator. Riboflavin, also known as vitamin B2, is naturally present in the body[64,65] and is thus biocompatible and suitable for *in vivo* applications[66]. Due to its biocompatibility, this photo-initiator is widely used in protein photo-crosslinking[67–70], and is shown to be suitable for light-patterning of reconstituted silk[22]. A key advantage over other photo-initiators is that the riboflavin chromophore absorbs strongly in the violet-blue part of the visible spectrum (between 400-500 nm)[69], enabling visible light to be used as opposed to previous works where UV light was utilised[16,71] which may result in further damage to the proteins[72,73].

After incorporation of riboflavin into the native silk solution and subsequent laser exposure, as described in the experimental section, a semi-solid pattern was obtained (Figure 1a,b). However, there is also the appearance of a secondary, sub-pixel, pattern with features below 5 μm in size (Figure 1c). This sub-pattern is most likely a result of the DMD mirror geometry and their spacing in the optical setup [74]. Interestingly these features produced a diffraction pattern under direct laser illumination (Figure 1d). This can be achieved by changing the distance between the elements of the pattern to generate specific diffraction patterns as a function of the light wavelength [11]. One potential use of such reflective patterns is for the fabrication of biocompatible implantable photonic devices [75] which can be used as specific sensors or electrodes [76], light delivery systems [77] and optical elements [78]. To investigate the potential of the native silk diffraction grids in similar applications, the glass slide with the photo-responsive solution was placed precisely at the focal point of the laser (0 mm), 8 mm below the focal point (-8 mm) and 8 mm above the focal point

(+8 mm). Fast Fourier Transform (FFT) performed on the images of the patterns indicated a shift with the variation in sample position. This confirms that precise sample alignment in PμSL allows to control the spacing of the sub-pixel patterns (Figure 1e). Since the total area of the projected patterns was about 1 cm^2, and the spacing between the sub-patterns was below 5 μm, this technique can be defined as being suitable for micro-patterning of silk on the micron scale.

This combination of silk's mechanical, biological and optical properties, combined with process/manufacturing flexibility and speed, make silk-PμSL fabricated patterns an idea candidate for range of applications. As the images are projected directly, there is practically unlimited design flexibility and elaborate silk-based photonic components can be realized in a few seconds (Figure 1f). Examples of such areas would be for the labelling of implants and medical devices[79–81] or in packaging in food industries[82]. As proof of concept, silk QR codes[83] were fabricated and after minimal image processing to enhance the contrast between the pattern and the background (Figure S1), the codes were readable by a commercially available QR Scanner installed on a mobile phone. Finally, pattern topography was analyzed by optical profilometry confirming that the patterns are raised above the surface with an average height of ~5 μm (Figure 1h).

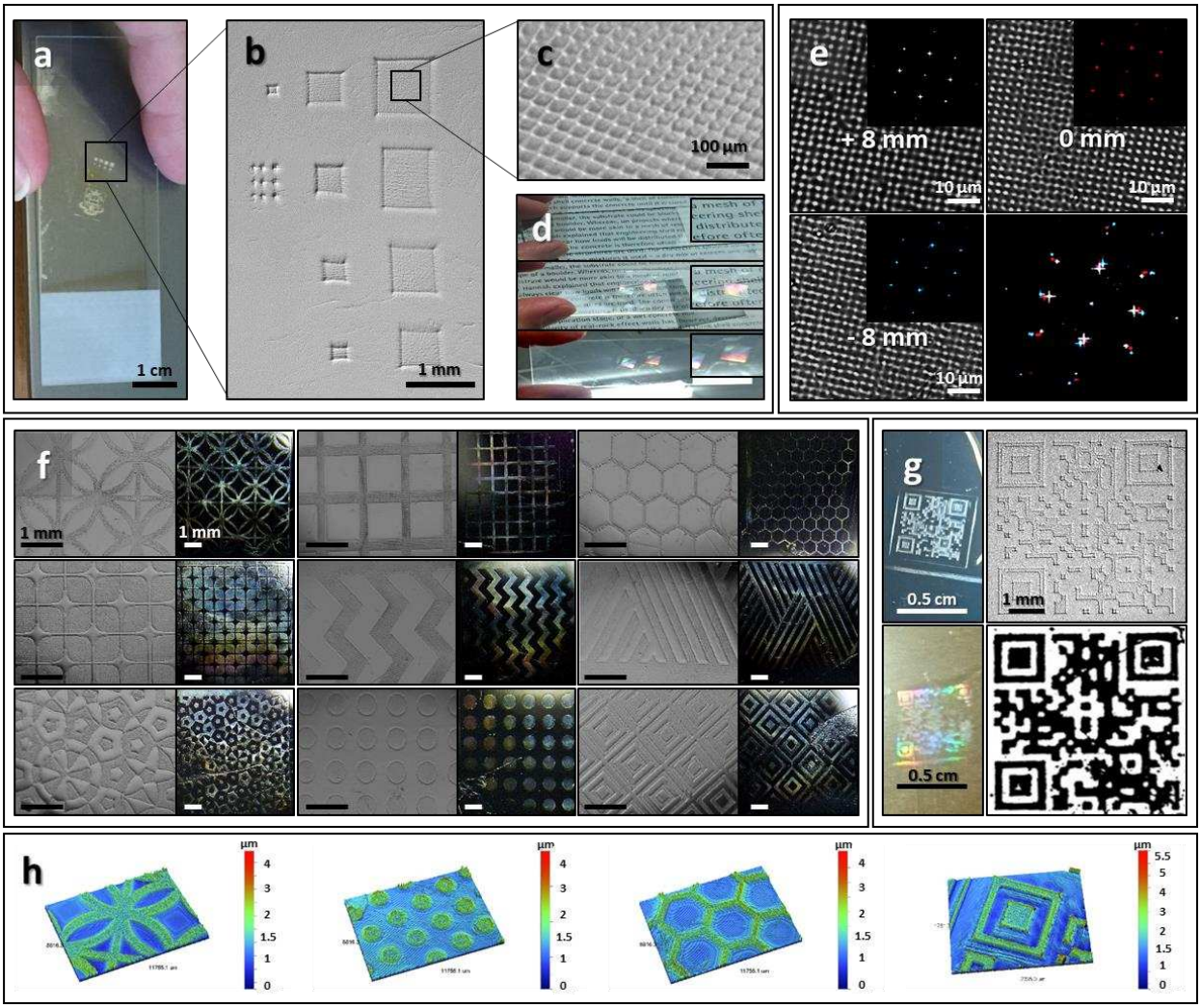

Figure 1: (a, b) Photograph and optical image of native silk patterns fabricated using projection micro stereo-lithography. (c) Secondary sub-pattern on the main pattern. (d) The patterns are transparent with light diffraction properties. (e) Optical microscopy image of the sub-patterns that were fabricated when the sample located at the focal point (top right), 8 mm above the focal point (top left) and 8 mm below the focal point (bottom left) of the laser. Inset show the FFT image of each sub-pattern. Overlay of the FFT images indicating that sample alignment allows control over the sub-patterns. (f) Optical images of native silk photonic components. (g) Silk QR code as fabricated and as appear after minimal image processing to make them suitable for scanning by QR code readers (bottom right). (h) Optical profilometry images of pattern topography.

Mechanism

Moving our attention towards investigating the mechanism behind this structuring process, previous studies have shown that protein solidification in the presence of light and photo cross-linker is usually attributed to chemical crosslinking of the protein[84]. Riboflavin, in particular, has been reported as a suitable photo cross-linker for many natural materials including collagen[67,68,85,86], alginate[87,88] and silk[22]. Such studies suggest that the key mechanism for riboflavin photo-gelation in silk and other proteins is attributed to the formation of di-tyrosine bonds[22,67,68,86]. This is because riboflavin absorbs UV, violet or blue light (350-500 nm) and acts as a type II photo-initiator where it extracts a proton from the hydroxyphenyl ring of the tyrosine[89] resulting in a cross-linking of 2 tyrosine moieties via the formation of a di-tyrosine bond[90]. However, during this process quenching reactions might also occur due to the presence of oxygen radicals, resulting in a recovery of the tyrosyl radicals and slowing down the reaction rate[91].

To validate the crosslinking mechanism, for our native silk PμSL system, the native protein solution, UV spectroscopy was employed to examine the tyrosine peak (275 nm) of native silk/riboflavin samples before and after exposure to laser light. Photo-exposed samples revealed a shoulder on the tyrosine peak which was not present in the spectra of the pure native silk solution or the riboflavin dye (Figure 2a). It is also interesting to note that the photocured sample does not show any peaks between 350-500 nm. This indicates that no direct cross-linking between the native silk and the dye has occurred and that the riboflavin was fully removed after washing with DI water. This in fact may have future utility in recycling of the photoinitiator or creating dye-free silk structures for tissue engineering applications. The shoulder on the main tyrosine peak was fitted, using peak fitting software (MagicPlot®) and a second peak was recognized (325 nm),

which was attributed to the presence of a di-tyrosine bonds[92] (Figure 2b). Those results confirm chemical cross-linking of the structure under laser illumination.

Further analysis of structure development was undertaken using Fourier-Transform Infrared spectroscopy (FTIR) to detect if there is any protein secondary structure conversions in the native silk after photo-curing. The typical structural conversion in silk associated with spinning can be characterized by a shift from the initial amide I peak position (~1650 cm^{-1})[93], indicating the formation of antiparallel β-sheet crystalline units which are present in silk fibers[94–98]. However, our FTIR analysis indicated a primarily amorphous structure of the photo-cured native silk patterns. This is particularly interesting as it means that structuring without conversion/crystallization of the native silk was achieved and our result agrees well with the literature[22,43], suggesting a different mechanism for silk photo-gelation, compared to native silk spinning[45] and methanol induced silk gelation[62]. However, this amorphous state endows additional flexibility as it is possible undertake further controlled conversion by washing the sample with MeOH (Figure S2). In fact, the level of crystallinity can be controlled by adjusting the concentration of MeOH/DI water solution and full conversion was measured after washing with MeOH solution above 50% v/v concentration. At concentrations >50% v/v, it was noted that this began to affect the gross morphological features of the film, with samples becoming rough and cloudy, with reduced optical properties upon exposure to 100% MeOH solution. Therefore, any future applications will inevitably have to trade-off optical properties vs. other properties, such as stiffness or biodegradability[2]. A deeper understanding of the microstructural changes of the silk upon photocuring and methanol addition can most likely be gained from further detailed analysis of the near infrared region[93] which will be investigated in the future.

As a final confirmation of chemical cross-linking in our system, silk-patterns were immersed in LiBr solution for 10 min at 60°C (a chaotropic agent known to solubilize silk through disruption of hydrogen bonds[40]). As expected, the photo-cured pattern remained stable while the non-exposed silk was fully dissolved (Figure 2c), confirming our findings regarding the stability of our system.

Mechanical characteristics

One of the challenges in many soft materials-based applications is to control mechanical properties[99–102]. Linking these insights into structure development with function, we then explored the effect of illumination on the stiffness (storage modulus, G′) of the native silk during and after the photocuring process. Using a rheometer equipped with an LED light source at the same wavelength as our PμSL setup, we performed in-situ measurements of the elastic modulus during constant illumination. All measurements began in darkness and illumination was applied after 300 s. After an induction period, significant increases in the values of G′ were recorded during illumination periods and the rate of modulus increase was proportional to the light flux irradiating the sample (Figure 2d). This suggests that by adjusting the light intensity, the number of riboflavin radicals that are being formed can be controlled and, as a result, direct control over the reaction rate can be achieved. The presence of an induction period may be attributed to several reasons such as crosslinking of other low molecular weight proteins naturally present in the silk duct[51], a period required for sufficient tyrosine radicals to form or the potential quenching effects of dissolved oxygen in the fibroin solution. To investigate the mechanical properties of the pre-fabricated silk patterns, the samples were exposed to laser light, dried and unexposed silk was removed by LiBr. Then, the samples were hydrated again prior to mechanical analysis. Subsequent dynamic shear analysis[103–106] of the patterns revealed an increase in the storage modulus with increase in energy dose projected to the sample. The maximum value was measured to be ~500 Pa

making the photo-cured silk significantly stiffer in compared to unexposed silk (~30 Pa) (Figure 2e). This value for native silk is higher by 200 Pa, compared to previous work when RS was used[22]. Furthermore, when patterns were post-treated with increasing concentrations (v/v) of MeOH solution, the storage modulus reached 2000 Pa for 50% and increased up to 16000 Pa for 100% solution (Figure 2f). Combining these results indicate that G′ of native silk/riboflavin patterns can be controlled over 4 orders of magnitude, thus replicating the mechanical properties of various human tissues such as brain (< 10^2 Pa), lungs (< 10^3 Pa), liver (10^3-10^4 Pa) and muscles (> 10^4 Pa) [107].

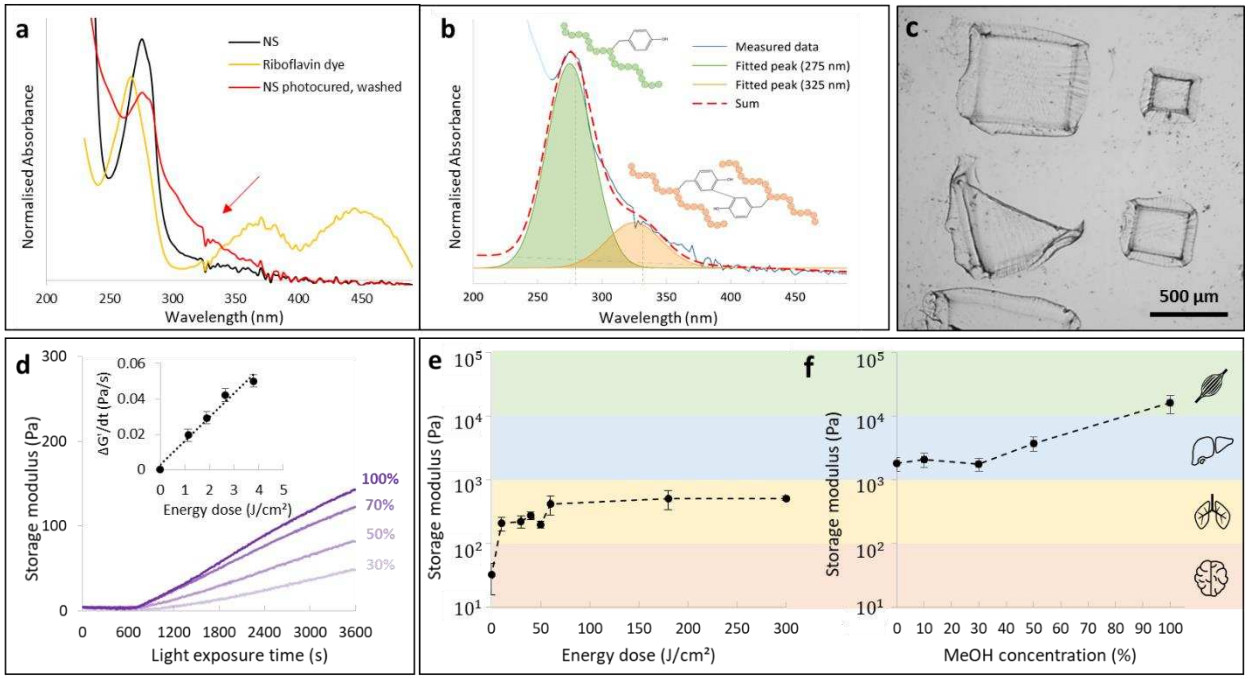

Figure 2: (a) UV-VIS spectra of native silk (black), riboflavin dye (yellow) and native silk after photocuring and removing of the riboflavin dye (red). Red arrow indicates the shoulder in the photocured sample. (b) Peak fitting of the photocured sample indicating the appearance of 325 nm peak corresponding to di-tyrosine bonds formation. (c) Silk pattern after wash with LiBr. Only the photocured areas remained while the non-exposed silk dissolved. (d) G' values over time as a

function of the light intensity. (Inset d) G' gradient as a function of the total energy dose. (e) Elastic modulus (G') value as a function of energy dose projected during pattern fabrication. (f) G' value as a function of MeOH concentration used to wash the sample post fabrication.

Protein quality

A wide range of publications show that photolithography is a suitable approach for protein patterning[21,86,108–114]. However, to unravel the influences of protein processing on pattern quality and complexity, we compared the performance of the reprocessed field standard RS protein against native silk. Given that the mechanism of the silk photo-gelation is dependent on di-tyrosine crosslinking, we hypothesised that to initiate the photo-gelation process, sufficient tyrosyl radicals need to be produced and therefore the concentration of the tyrosine in the solution, the light intensity applied, and the chain lengths of the polymers combined will ultimately determine the crosslinking rate and the final quality of the pattern. As a further means to test this hypothesis we introduced a control of a tyrosine-rich polymer which has the potential to form 25 times more di-tyrosine bonds than silk but is of a lower molecular weight.

Two different images were projected onto riboflavin containing native silk, RS and poly(Glu-co-Tyr) solutions. Minimum feature size was tested by a grid pattern with patterns ranging from 4·4 pixel^2 to 100·100 pixel^2 squares (Figure 3a-c, top). The quality of the image was tested by projecting the pattern of the University of Sheffield logo (Figure 3a-c, bottom). For each sample type, the lowest concentration which provided the best pattern was selected. Image quality was assessed by a quantitative parameter of Similarity between the original image projected from the DMD and the resulting pattern (see Figure 3S in supplementary data).

We report that native silk offered a minimum feature size of 40 μm and the highest Similarity of 80% (Figure 3d, e) at just 1 wt% concentration. This concentration was found to be at least 2.5 times lower than any reconstituted silk solution used for photo-fabrication in the currently reported literature[26–28,43,115,116] and 6 times lower than the RS/fibroin photocurable resin recently reported by Applegate *at al.*[22]. Furthermore, by using native silk we managed to produce images with a similarity index >75% at all tested concentrations (0.5-3 wt%). Hence, we conclude that the suitability of a protein for a compound image fabrication is not solely a factor of the protein concentration. This is also supported by the lower quality image received for poly(Glu-co-Tyr) despite the high concentration of tyrosine units in the sample (1.25 mol %) compared to native silk solution (0.05 mol %).

The performance improvement of native silk compared to the other samples is therefore most likely a result of its higher molecular weight. To confirm this hypothesis, gel electrophoresis demonstrated that the Mw of native silk (≥ 420 kDa) was significantly higher than that of the reconstituted silk used (≤ 250 kDa) (see Figure S4). The degradation of silk proteins during reconstitution is attributed not to the LiBr resolubilization step but the degumming process. Degumming has been clearly shown to reduce silk's molecular weight with exposure time and concentration of Na_2CO_3[6,45,117,118], something we confirmed through comparison of image quality using silk solutions prepared with differing concentrations of Na_2CO_3 (Figure 3g). In addition, we noticed that chemical degumming significantly reduced the stiffness of our RS material, obtaining less than 50% of the values for a non-degummed RS sample (Figure S5). In summary our findings are in good agreement with the wider photo-lithography literature which has previously shown a decrease in feature size with the increase of the molecular weight of the polymer[119,120].

These results strongly suggest that process of reconstitution and thus the quality of the resulting protein solution, significantly effects the potential applications of photo-patterning and printing in silk. However, whilst native silk is a convenient gold standard, it is not really an industrially scalable alternative as it has to be manually extracted from the animal, which is both time-consuming and technically challenging, therefore we are currently placing our efforts towards first understanding the nuances and then the development of improved, scalable reconstitution protocols.

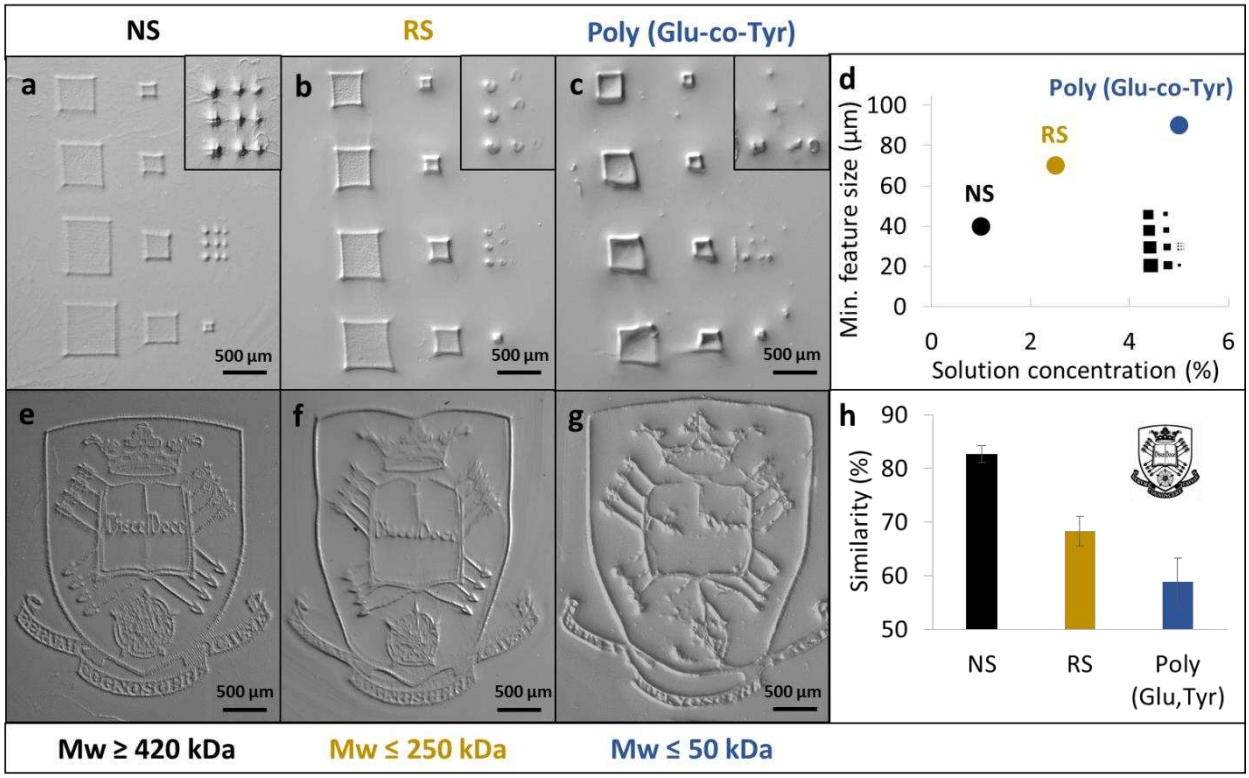

Figure 3: Comparison between grid pattern (to evaluate feature size) and University of Sheffield logo patterns (to evaluate image quality) as received for (a,g) native silk, (b,f) reconstituted silk (RS), (c,g) Poly (Glu-co-Tyr) protein. (d) Minimal visible feature size as a function of optimal solution concentration. (h) Similarity value of the fabricated pattern to the projected image.

CONCLUSIONS

In this work, we have demonstrated that native silk is not only suitable for photo-lithography, but also enables us to achieve patterns with smaller feature size, better image quality and at lower concentrations when compared to a standard reconstituted silk. Patterns down to 40 μm were fabricated, presenting an improvement of 20 % compared to previously reported riboflavin/RS photocuring [22]. By using PμSL method, photonic components were produced alongside larger scale patterns such as readable QR codes. We also introduced, for the first time, the Similarity value to assess image quality in addition to feature size, for a better comparison between various structuring technique and materials. Furthermore, the mechanism behind native silk photo-gelation was explored, with our findings supporting previous studies that suggested the formation of di-tyrosine bonds and chemical cross-linking of the protein.

However, we also report that no protein structural conversion (β-sheet formation) occurred during the photo-curing of native silk, allowing us to decouple structuring with conversion and opening up the possibility to control protein crystallinity and mechanical properties. Finally, by comparing native silk to reconstituted silk, we propose that molecular weight is the main parameter contributing to the quality of the fabricated image and the mechanical stiffness of a silk patterns. As a result, we propose that to allow a fair comparison between various light-based structuring techniques in the future, that protein molecular weight should be provided in addition to protein concentration.

In conclusion, we believe that our approach towards silk pattern generation and the insights gained into light-based silk structuring can hopefully contribute towards both a fundamental understanding of natural silk solidification and potentially find application in food, packaging, security marking and medical devices industries in the future.

Author Contributions

AB and PL performed the experimentation, all authors contributed to writing of the manuscript. All authors have given approval to the final version of the manuscript.

Funding Sources

EPSRC, project reference EP/K005693/1

EPSRC, project reference EP/I007695/1

MRC, project reference MR/L012669/1

ACKNOWLEDGMENT

FC and AB thank the University of Sheffield for funding of a University Prize Scholarship and PL and CH thank EPSRC for funding under (SPICE, project reference EP/K005693/1). FC acknowledges funding from the EPSRC (Grant No. EP/I007695/1) and the Medical Research Council (MR/L012669/1) for funding the equipment used in this study.

SUPPORTING INFORMATION STATEMENT

Supporting information contains 5 figures.
Figure S1 demonstrates native silk pattern before and after image processing.
Figure S2 demonstrates the effect of methanol wash on silk crystallization
Figure S3 demonstrates the process image similarity calculation
Figure S4 shows gel electrophoresis results
Figure S5 compares the photopolymerisation rate of native and RS and demonstrates the effect of RS degumming process on elastic modulus of the silk.

REFERENCES

(1) Belanger, W. A. The Silk Road in World History. By Xinru Liu. Oxford: Oxford University

Press, 2010, 168 Pp. *J. Asian Stud.* **2011**, *70* (04), 1156–1157.

(2) Holland, C.; Numata, K.; Rnjak-Kovacina, J.; Seib, F.P.; The Biomedical use of silk: Past, Present, Future. *Adv. Health. Mater.* **2019** *8 (1),* 1800465 https://doi.org/10.1002/adhm.201800465

(3) Moy, R. L.; Waldman, B.; Hein, D. W. A Review of Sutures and Suturing Techniques. *J. Dermatol. Surg. Oncol.* **1992**, *18* (9), 785–795. https://doi.org/10.1111/j.1524-4725.1992.tb03036.x.

(4) Koeppel, A.; Holland, C. Progress and Trends in Artificial Silk Spinning: A Systematic Review. *ACS Biomater. Sci. Eng.* **2017**, *3* (3), 226–237. https://doi.org/10.1021/acsbiomaterials.6b00669.

(5) Kasoju, N.; Bora, U. Silk Fibroin in Tissue Engineering. *Adv. Healthc. Mater.* **2012**, *1* (4), 393–412. https://doi.org/10.1002/adhm.201200097.

(6) Rockwood, D. N.; Preda, R. C.; Yücel, T.; Wang, X.; Lovett, M. L.; Kaplan, D. L. Materials Fabrication from Bombyx Mori Silk Fibroin. *Nat. Protoc.* **2011**, *6* (September), 1612–1631. https://doi.org/10.1038/nprot.2011.379.

(7) Lawrence, B. D.; Marchant, J. K.; Pindrus, M. a.; Omenetto, F. G.; Kaplan, D. L. Silk Film Biomaterials for Cornea Tissue Engineering. *Biomaterials* **2009**, *30* (7), 1299–1308. https://doi.org/10.1016/j.biomaterials.2008.11.018.

(8) Madduri, S.; Papaloïzos, M.; Gander, B. Trophically and Topographically Functionalized Silk Fibroin Nerve Conduits for Guided Peripheral Nerve Regeneration. *Biomaterials* **2010**,

31 (8), 2323–2334. https://doi.org/10.1016/j.biomaterials.2009.11.073.

(9) Tsioris, K.; Raja, W. K.; Pritchard, E. M.; Panilaitis, B.; Kaplan, D. L.; Omenetto, F. G. Fabrication of Silk Microneedles for Controlled-Release Drug Delivery. *Adv. Funct. Mater.* **2012**, *22* (2), 330–335. https://doi.org/10.1002/adfm.201102012.

(10) Omenetto, F. G.; Kaplan, D. L. A New Route for Silk. *Nat Phot.* **2008**, *2* (11), 641–643.

(11) Kim, S.; Marelli, B.; Brenckle, M. A.; Mitropoulos, A. N.; Gil, E.-S.; Tsioris, K.; Tao, H.; Kaplan, D. L.; Omenetto, F. G. All-Water-Based Electron-Beam Lithography Using Silk as a Resist. *Nat Nano* **2014**, *9* (4), 306–310.

(12) Kim, D.-H.; Viventi, J.; Amsden, J. J.; Xiao, J.; Vigeland, L.; Kim, Y.-S.; Blanco, J. A.; Panilaitis, B.; Frechette, E. S.; Contreras, D.; Kaplan, D. L.; Omenetto, F. G.; Huang, Y.; Hwang, K.-C.; Zakin, M. R.; Litt, B.; Rogers, J. A. Dissolvable Films of Silk Fibroin for Ultrathin Conformal Bio-Integrated Electronics. *Nat Mater* **2010**, *9* (6), 511–517.

(13) Feng, L.; Li, S.; Li, Y.; Li, H.; Zhang, L.; Zhai, J.; Song, Y.; Liu, B.; Jiang, L.; Zhu, D. Super-Hydrophobic Surfaces: From Natural to Artificial. *Adv. Mater.* **2002**, *14* (24), 1857–1860. https://doi.org/10.1002/adma.200290020.

(14) Craighead, H. .; James, C. .; Turner, A. M. . Chemical and Topographical Patterning for Directed Cell Attachment. *Curr. Opin. Solid State Mater. Sci.* **2001**, *5* (2), 177–184. https://doi.org/10.1016/S1359-0286(01)00005-5.

(15) Kong, X. D.; Cui, F. Z.; Wang, X. M.; Zhang, M.; Zhang, W. Silk Fibroin Regulated Mineralization of Hydroxyapatite Nanocrystals. *J. Cryst. Growth* **2004**, *270* (1–2), 197–

202. https://doi.org/10.1016/j.jcrysgro.2004.06.007.

(16) Pal, R. K.; Kurland, N. E.; Wang, C.; Kundu, S. C.; Yadavalli, V. K. Biopatterning of Silk Proteins for Soft Micro-Optics. *ACS Appl. Mater. Interfaces* **2015**, *7* (16), 8809–8816. https://doi.org/10.1021/acsami.5b01380.

(17) Shimanovich, U.; Pinotsi, D.; Shimanovich, K.; Yu, N.; Bolisetty, S.; Adamcik, J.; Mezzenga, R.; Charmet, J.; Vollrath, F.; Gazit, E.; Dobson, C. M.; Schierle, G. K.; Holland, C.; Kaminski, C. F.; Knowles, T. P. J. Biophotonics of Native Silk Fibrils. *Macromol. Biosci.* n/a-n/a. https://doi.org/10.1002/mabi.201700295.

(18) Kim, S.; Mitropoulos, A. N.; Spitzberg, J. D.; Tao, H.; Kaplan, D. L.; Omenetto, F. G. Silk Inverse Opals. *Nat Phot.* **2012**, *6* (12), 818–823.

(19) Galeotti, F.; Andicsová, A.; Yunus, S.; Botta, C. *Precise Surface Patterning of Silk Fibroin Films by Breath Figures*; 2012; Vol. 8. https://doi.org/10.1039/C2SM25089F.

(20) Amsden, J. J.; Domachuk, P.; Gopinath, A.; White, R. D.; Negro, L. D.; Kaplan, D. L.; Omenetto, F. G. Rapid Nanoimprinting of Silk Fibroin Films for Biophotonic Applications. *Adv. Mater.* **2010**, *22* (15), 1746–1749. https://doi.org/10.1002/adma.200903166.

(21) Kurland, N. E.; Dey, T.; Kundu, S. C.; Yadavalli, V. K. Precise Patterning of Silk Microstructures Using Photolithography. *Adv. Mater.* **2013**, *25* (43), 6207–6212. https://doi.org/10.1002/adma.201302823.

(22) Applegate, M. B.; Partlow, B. P.; Coburn, J.; Marelli, B.; Pirie, C.; Pineda, R.; Kaplan, D. L.; Omenetto, F. G. Photocrosslinking of Silk Fibroin Using Riboflavin for Ocular

Prostheses. *Adv. Mater.* **2016**, *28* (12), 2417–2420. https://doi.org/10.1002/adma.201504527.

(23) Ramendra, K. P.; Ahmed, A. F.; Maryanne, M. C.; Subhas, C. K.; Vamsi, K. Y. Photolithographic Micropatterning of Conducting Polymers on Flexible Silk Matrices. *Adv. Mater.* **2015**, *28* (7), 1406–1412. https://doi.org/10.1002/adma.201504736.

(24) Qin, N.; Zhang, S.; Jiang, J.; Corder, S. G.; Qian, Z.; Zhou, Z.; Lee, W.; Liu, K.; Wang, X.; Li, X.; Shi, Z.; Mao, Y.; Bechtel, H. A.; Martin, M. C.; Xia, X.; Marelli, B.; Kaplan, D. L.; Omenetto, F. G.; Liu, M.; et al. Nanoscale Probing of Electron-Regulated Structural Transitions in Silk Proteins by near-Field IR Imaging and Nano-Spectroscopy. **2016**, *7*, 13079.

(25) Wray LS, Rnjak-Kovacina J, Mandal BB, Schmidt DF, Gil ES, K. D. A Silk-Based Scaffold Platform with Tunable Architecture for Engineering Critically-Sized Tissue Constructs. *Biomaterials* **2012**, *33* (36), 9214–9224. https://doi.org/10.1016/J.BIOMATERIALS.2012.09.017.

(26) Sun, Y.-L.; Li, Q.; Sun, S.-M.; Huang, J.-C.; Zheng, B.-Y.; Chen, Q.-D.; Shao, Z.-Z.; Sun, H.-B. Aqueous Multiphoton Lithography with Multifunctional Silk-Centred Bio-Resists. *Nat. Commun.* **2015**, *6*.

(27) Dickerson, M. B.; Dennis, P. B.; Tondiglia, V. P.; Nadeau, L. J.; Singh, K. M.; Drummy, L. F.; Partlow, B. P.; Brown, D. P.; Omenetto, F. G.; Kaplan, D. L.; Naik, R. R. 3D Printing of Regenerated Silk Fibroin and Antibody-Containing Microstructures via Multiphoton Lithography. *ACS Biomater. Sci. Eng.* **2017**, *3* (9), 2064–2075.

https://doi.org/10.1021/acsbiomaterials.7b00338.

(28) Whittaker, J. L.; Choudhury, N. R.; Dutta, N. K.; Zannettino, A. Facile and Rapid Ruthenium Mediated Photo-Crosslinking of Bombyx Mori Silk Fibroin. *J. Mater. Chem. B* **2014**, *2* (37), 6259–6270. https://doi.org/10.1039/C4TB00698D.

(29) Hull, C. W. Apparatus for Production of Three-Dimensional Objects by Stereolithography. Google Patents March 11, 1986.

(30) Jacobs, P. F. *Rapid Prototyping & Manufacturing: Fundamentals of Stereolithography*; Society of Manufacturing Engineers, 1992.

(31) Lee, M. P.; Cooper, G. J. T.; Hinkley, T.; Gibson, G. M.; Padgett, M. J.; Cronin, L. Development of a 3D Printer Using Scanning Projection Stereolithography. *Sci. Rep.* **2015**, *5*.

(32) Pan, Y.; Zhou, C.; Chen, Y. A Fast Mask Projection Stereolithography Process for Fabricating Digital Models in Minutes. *J. Manuf. Sci. Eng.* **2012**, *134* (5), 51011–51019.

(33) Chia, H. N.; Wu, B. M. Recent Advances in 3D Printing of Biomaterials. *J. Biol. Eng.* **2015**, *9* (1), 4. https://doi.org/10.1186/s13036-015-0001-4.

(34) Melchels, F. P. W.; Feijen, J.; Grijpma, D. W. A Review on Stereolithography and Its Applications in Biomedical Engineering. *Biomaterials* **2010**, *31* (24), 6121–6130. https://doi.org/10.1016/j.biomaterials.2010.04.050.

(35) Pateman, C. J.; Harding, A. J.; Glen, A.; Taylor, C. S.; Christmas, C. R.; Robinson, P. P.; Rimmer, S.; Boissonade, F. M.; Claeyssens, F.; Haycock, J. W. Nerve Guides Manufactured

from Photocurable Polymers to Aid Peripheral Nerve Repair. *Biomaterials* **2015**, *49*, 77–89. https://doi.org/https://doi.org/10.1016/j.biomaterials.2015.01.055.

(36) Sun, C.; Fang, N.; Wu, D. M.; Zhang, X. Projection Micro-Stereolithography Using Digital Micro-Mirror Dynamic Mask. *Sensors Actuators A Phys.* **2005**, *121* (1), 113–120. https://doi.org/https://doi.org/10.1016/j.sna.2004.12.011.

(37) Bandelier, P.; Charley, A.-L.; Lagrange, A. Photolithography. In *Lithography*; John Wiley & Sons, Inc., 2013; pp 1–40. https://doi.org/10.1002/9781118557662.ch1.

(38) Ikuta, K.; Maruo, S.; Kojima, S. New Micro Stereo Lithography for Freely Movable 3D Micro Structure-Super IH Process with Submicron Resolution. In *Proceedings MEMS 98. IEEE. Eleventh Annual International Workshop on Micro Electro Mechanical Systems. An Investigation of Micro Structures, Sensors, Actuators, Machines and Systems (Cat. No.98CH36176*; 1998; pp 290–295. https://doi.org/10.1109/MEMSYS.1998.659770.

(39) Pan, Y.; Dagli, C. Dynamic Resolution Control in a Laser Projection-Based Stereolithography System. *Rapid Prototyp. J.* **2017**, *23* (1), 190–200. https://doi.org/10.1108/RPJ-08-2015-0113.

(40) Rockwood, D. N.; Preda, R. C.; Yucel, T.; Wang, X.; Lovett, M. L.; Kaplan, D. L. Materials Fabrication from Bombyx Mori Silk Fibroin. *Nat. Protoc.* **2011**, *6* (10), 1612–1631.

(41) Partlow, B. P.; Tabatabai, A. P.; Leisk, G. G.; Cebe, P.; Blair, D. L.; Kaplan, D. L. Silk Fibroin Degradation Related to Rheological and Mechanical Properties. *Macromol. Biosci.* **2016**, *16* (5), 666–675. https://doi.org/10.1002/mabi.201500370.

(42) Kim, H. H.; Song, D. W.; Kim, M. J.; Ryu, S. J.; Um, I. C.; Ki, C. S.; Park, Y. H. Effect of Silk Fibroin Molecular Weight on Physical Property of Silk Hydrogel. *Polymer (Guildf).* **2016**, *90* (Supplement C), 26–33. https://doi.org/https://doi.org/10.1016/j.polymer.2016.02.054.

(43) Maximova, K.; Wang, X.; Balčytis, A.; Fan, L.; Li, J.; Juodkazis, S. Silk Patterns Made by Direct Femtosecond Laser Writing. *Biomicrofluidics* **2016**, *10* (5). https://doi.org/10.1063/1.4962294.

(44) Holland, C.; Porter, D.; Vollrath, F. Comparing the Rheology of Mulberry and "Wild" Silkworm Spinning Dopes. *Biopolymers* **2012**, *97* (6), 362–367. https://doi.org/10.1002/bip.22011.

(45) Holland, C.; Terry, A. E.; Porter, D.; Vollrath, F. *Natural and Unnatural Silks*; 2007; Vol. 48. https://doi.org/10.1016/j.polymer.2007.04.019.

(46) Hou, Y.; Xia, Q.; Zhao, P.; Zou, Y.; Liu, H.; Guan, J.; Gong, J.; Xiang, Z. Studies on Middle and Posterior Silk Glands of Silkworm (Bombyx Mori) Using Two-Dimensional Electrophoresis and Mass Spectrometry. *Insect Biochem. Mol. Biol.* **2007**, *37* (5), 486–496. https://doi.org/10.1016/j.ibmb.2007.02.011.

(47) Sparkes, J.; Holland, C. Analysis of the Pressure Requirements for Silk Spinning Reveals a Pultrusion Dominated Process. *Nat. Commun.* **2017**, *8* (1), 594. https://doi.org/10.1038/s41467-017-00409-7.

(48) Laity, P. R.; Gilks, S. E.; Holland, C. Rheological Behaviour of Native Silk Feedstocks. *Polymer (Guildf).* **2015**, *67*, 28–39. https://doi.org/10.1016/j.polymer.2015.04.049.

(49) Holland, C.; Terry, A. E.; Porter, D.; Vollrath, F. Comparing the Rheology of Native Spider and Silkworm Spinning Dope. *Nat Mater* **2006**, *5* (11), 870–874.

(50) Laity, R. P.; Holland, C. The Rheology behind Stress-Induced Solidification in Native Silk Feedstocks. *International Journal of Molecular Sciences* . 2016. https://doi.org/10.3390/ijms17111812.

(51) Laity, P. R.; Holland, C. Native Silk Feedstock as a Model Biopolymer: A Rheological Perspective. *Biomacromolecules* **2016**, *17* (8), 2662–2671. https://doi.org/10.1021/acs.biomac.6b00709.

(52) Porter, D.; Vollrath, F. Silk as a Biomimetic Ideal for Structural Polymers. *Adv. Mater.* **2009**, *21* (4), 487–492. https://doi.org/10.1002/adma.200801332.

(53) Shimanovich, U.; Ruggeri, F. S.; De Genst, E.; Adamcik, J.; Barros, T. P.; Porter, D.; Müller, T.; Mezzenga, R.; Dobson, C. M.; Vollrath, F.; Holland, C.; Knowles, T. P. J. Silk Micrococoons for Protein Stabilisation and Molecular Encapsulation. *Nat. Commun.* **2017**, *8*, 15902.

(54) MACHIDA, J. On the Secretion of the Silk Substances of the Silkworm. *Proc. Imp. Acad.* **2018**, *2* (8), 421–422. https://doi.org/10.2183/pjab1912.2.421.

(55) Akai, H. The Structure and Ultrastructure of the Silk Gland. *Experientia* **1983**, *39* (5), 443–449. https://doi.org/10.1007/BF01965158.

(56) Hu, X.; Shmelev, K.; Sun, L.; Gil, E.-S.; Park, S.-H.; Cebe, P.; Kaplan, D. L. Regulation of Silk Material Structure by Temperature-Controlled Water Vapor Annealing.

Biomacromolecules **2011**, *12* (5), 1686–1696. https://doi.org/10.1021/bm200062a.

(57) Askarieh, G.; Hedhammar, M.; Nordling, K.; Saenz, A.; Casals, C.; Rising, A.; Johansson, J.; Knight, S. D. Self-Assembly of Spider Silk Proteins Is Controlled by a PH-Sensitive Relay. *Nature* **2010**, *465* (7295), 236–238.

(58) Terry, A. E.; Knight, D. P.; Porter, D.; Vollrath, F. PH Induced Changes in the Rheology of Silk Fibroin Solution from the Middle Division of Bombyx Mori Silkworm. *Biomacromolecules* **2004**, *5* (3), 768–772. https://doi.org/10.1021/bm034381v.

(59) Ayub, Z. H.; Hirabayashi, K.; Arai, M. EFFECT OF PH ON SILK FIBROIN GELATION. *Sen'i Gakkaishi* **1992**, *48* (3), 141–144. https://doi.org/10.2115/fiber.48.3_141.

(60) Holland, C.; Urbach, J. S.; Blair, D. L. Direct Visualization of Shear Dependent Silk Fibrillogenesis. *Soft Matter* **2012**, *8* (9), 2590–2594. https://doi.org/10.1039/C2SM06886A.

(61) Wang, X.; Kluge, J. A.; Leisk, G. G.; Kaplan, D. L. Sonication-Induced Gelation of Silk Fibroin for Cell Encapsulation. *Biomaterials* **2008**, *29* (8), 1054–1064. https://doi.org/https://doi.org/10.1016/j.biomaterials.2007.11.003.

(62) Tsukada, M.; Gotoh, Y.; Nagura, M.; Minoura, N.; Kasai, N.; Freddi, G. Structural Changes of Silk Fibroin Membranes Induced by Immersion in Methanol Aqueous Solutions. *J. Polym. Sci. Part B Polym. Phys.* **1994**, *32* (5), 961–968.

(63) Nagarkar, S.; Nicolai, T.; Chassenieux, C.; Lele, A. Structure and Gelation Mechanism of Silk Hydrogels. *Phys. Chem. Chem. Phys.* **2010**, *12* (15), 3834–3844. https://doi.org/10.1039/B916319K.

(64) Ball, G. F. M. *Vitamins: Their Role in the Human Body*; John Wiley & Sons, 2008.

(65) Wurtman, R. J. The Effects of Light on the Human Body. *Sci. Am.* **1975**, *233* (1), 68–77.

(66) FDA. *Select Committee on GRAS Substances (SCOGS) Opinion: Riboflavin, Riboflavin-5'-Phosphate*; New Hampshire Avenue Silver Spring, MD, 1979.

(67) Kato, Y.; Uchida, K.; Kawakishi, S. AGGREGATION OF COLLAGEN EXPOSED TO UVA IN THE PRESENCE OF RIBOFLAVIN: A PLAUSIBLE ROLE OF TYROSINE MODIFICATION. *Photochem. Photobiol.* **1994**, *59* (3), 343–349. https://doi.org/10.1111/j.1751-1097.1994.tb05045.x.

(68) Wollensak, G.; Wilsch, M.; Spoerl, E.; Seiler, T. Collagen Fiber Diameter in the Rabbit Cornea After Collagen Crosslinking by Riboflavin/UVA. *Cornea* **2004**, *23* (5).

(69) Galston, A. W.; Baker, R. S. Studies on the Physiology of Light Action. II. The Photodynamic Action of Riboflavin. *Am. J. Bot.* **1949**, 773–780.

(70) Wollensak, G.; Spoerl, E. *Collagen Crosslinking of Human and Porcine Sclera*; 2004; Vol. 30. https://doi.org/10.1016/j.jcrs.2003.11.032.

(71) Periolatto, M.; Ferrero, F.; Vineis, C. Antimicrobial Chitosan Finish of Cotton and Silk Fabrics by UV-Curing with 2-Hydroxy-2-Methylphenylpropane-1-One. *Carbohydr. Polym.* **2012**, *88* (1), 201–205. https://doi.org/https://doi.org/10.1016/j.carbpol.2011.11.093.

(72) Sionkowska, A.; Planecka, A. The Influence of UV Radiation on Silk Fibroin. *Polym. Degrad. Stab.* **2011**, *96* (4), 523–528. https://doi.org/https://doi.org/10.1016/j.polymdegradstab.2011.01.001.

(73) Abaskharon, R. M.; Gai, F. Direct Measurement of the Tryptophan-Mediated Photocleavage Kinetics of a Protein Disulfide Bond. *Phys. Chem. Chem. Phys.* **2016**, *18* (14), 9602–9607.

(74) Texas Instruments. *DMD Product Preview Data Sheete*; 2005.

(75) Humar, M.; Kwok, S. J. J.; Choi, M.; Yetisen, A. K.; Cho, S.; Yun, S. H. Toward Biomaterial-Based Implantable Photonic Devices. *Nanophotonics* **2017**, *6* (2), 414–434. https://doi.org/10.1515/nanoph-2016-0003.

(76) Jiang, L.-C.; Zhang, W.-D. A Highly Sensitive Nonenzymatic Glucose Sensor Based on CuO Nanoparticles-Modified Carbon Nanotube Electrode. *Biosens. Bioelectron.* **2010**, *25* (6), 1402–1407. https://doi.org/https://doi.org/10.1016/j.bios.2009.10.038.

(77) Slinger, C.; Cameron, C.; Stanley, M. Computer-Generated Holography as a Generic Display Technology. *Computer (Long. Beach. Calif).* **2005**, *38* (8), 46–53. https://doi.org/10.1109/MC.2005.260.

(78) Lin, D.; Fan, P.; Hasman, E.; Brongersma, M. L. Dielectric Gradient Metasurface Optical Elements. *Science (80-.).* **2014**, *345* (6194), 298 LP – 302.

(79) Cerveny, D. Systems, Methods, and Apparatus for Integrating Scannable Codes in Medical Devices. Google Patents September 18, 2014.

(80) Czuszynski, K.; Ruminski, J. Interaction with Medical Data Using QR-Codes. In *2014 7th International Conference on Human System Interactions (HSI)*; 2014; pp 182–187. https://doi.org/10.1109/HSI.2014.6860471.

(81) Han, S.; Bae, H. J.; Kim, J.; Shin, S.; Choi, S.-E.; Lee, S. H.; Kwon, S.; Park, W. Lithographically Encoded Polymer Microtaggant Using High-Capacity and Error-Correctable QR Code for Anti-Counterfeiting of Drugs. *Adv. Mater.* **2012**, *24* (44), 5924–5929. https://doi.org/10.1002/adma.201201486.

(82) Marelli, B.; Brenckle, M. A.; Kaplan, D. L.; Omenetto, F. G. Silk Fibroin as Edible Coating for Perishable Food Preservation. *Sci. Rep.* **2016**, *6* (November 2015), 1–11. https://doi.org/10.1038/srep25263.

(83) Hara, M. Method for Displaying and Reading Information Code for Commercial Transaction. Google Patents February 14, 2006.

(84) Partlow, B. P.; Applegate, M. B.; Omenetto, F. G.; Kaplan, D. L. Dityrosine Cross-Linking in Designing Biomaterials. *ACS Biomater. Sci. Eng.* **2016**, *2* (12), 2108–2121. https://doi.org/10.1021/acsbiomaterials.6b00454.

(85) Wollensak, G.; Spoerl, E.; Seiler, T. Riboflavin/Ultraviolet-A–Induced Collagen Crosslinking for the Treatment of Keratoconus. *Am. J. Ophthalmol.* **2003**, *135* (5), 620–627.

(86) Heo, J.; Koh, R. H.; Shim, W.; Kim, H. D.; Yim, H.-G.; Hwang, N. S. Riboflavin-Induced Photo-Crosslinking of Collagen Hydrogel and Its Application in Meniscus Tissue Engineering. *Drug Deliv. Transl. Res.* **2016**, *6* (2), 148–158. https://doi.org/10.1007/s13346-015-0224-4.

(87) Baldursdóttir, S. G.; Kjøniksen, A.-L.; Karlsen, J.; Nyström, B.; Roots, J.; Tønnesen, H. H. Riboflavin-Photosensitized Changes in Aqueous Solutions of Alginate. Rheological

Studies. *Biomacromolecules* **2003**, *4* (2), 429–436.

(88) White, J. C.; Stoppel, W. L.; Roberts, S. C.; Bhatia, S. R. Addition of Perfluorocarbons to Alginate Hydrogels Significantly Impacts Molecular Transport and Fracture Stress. *J. Biomed. Mater. Res. Part A* **2013**, *101* (2), 438–446.

(89) Edwards, A. M.; Silva, E. Effect of Visible Light on Selected Enzymes, Vitamins and Amino Acids. *J. Photochem. Photobiol. B Biol.* **2001**, *63* (1), 126–131.

(90) Bhatia, J.; Stegink, L. D.; Ziegler, E. E. Riboflavin Enhances Photo-Oxidation of Amino Acids under Simulated Clinical Conditions. *J. Parenter. Enter. Nutr.* **1983**, *7* (3), 277–279.

(91) Hunter, E. P. L.; Desrosiers, M. F.; Simic, M. G. The Effect of Oxygen, Antioxidants, and Superoxide Radical on Tyrosine Phenoxyl Radical Dimerization. *Free Radic. Biol. Med.* **1989**, *6* (6), 581–585.

(92) Correia, M.; Neves-Petersen, M. T.; Jeppesen, P. B.; Gregersen, S.; Petersen, S. B. UV-Light Exposure of Insulin: Pharmaceutical Implications upon Covalent Insulin Dityrosine Dimerization and Disulphide Bond Photolysis. *PLoS One* **2012**, *7* (12), e50733. https://doi.org/10.1371/journal.pone.0050733.

(93) Balčytis, A.; Ryu, M.; Wang, X.; Novelli, F.; Seniutinas, G.; Du, S.; Wang, X.; Li, J.; Davis, J.; Appadoo, D.; Morikawa, J.; Juodkazis, S. Silk: Optical Properties over 12.6 Octaves THz-IR-Visible-UV Range. *Materials* . 2017. https://doi.org/10.3390/ma10040356.

(94) Ohgo, K.; Bagusat, F.; Asakura, T.; Scheler, U. Investigation of Structural Transition of Regenerated Silk Fibroin Aqueous Solution by Rheo-NMR Spectroscopy Investigation of

Structural Transition of Regenerated Silk Fibroin Aqueous Solution by Rheo-NMR Spectroscopy. *Biomacromolecules* **2008**, No. 3, 4182–4186. https://doi.org/10.1021/ja710011d.

(95) Boulet-Audet, M.; Lefèvre, T.; Buffeteau, T.; Pézolet, M. Attenuated Total Reflection Infrared Spectroscopy: An Efficient Technique to Quantitatively Determine the Orientation and Conformation of Proteins in Single Silk Fibers. *Appl. Spectrosc.* **2008**, *62* (9), 956–962. https://doi.org/10.1366/000370208785793380.

(96) Boulet-Audet, M.; Vollrath, F.; Holland, C. Identification and Classification of Silks Using Infrared Spectroscopy. *J. Exp. Biol.* **2015**, *218* (19), 3138–3149.

(97) Chen, X.; Knight, D. P.; Shao, Z.; Vollrath, F. Regenerated Bombyx Silk Solutions Studied with Rheometry and FTIR. *Polymer (Guildf).* **2001**, *42* (25), 9969–9974. https://doi.org/10.1016/S0032-3861(01)00541-9.

(98) Boulet-Audet, M.; Terry, A. E.; Vollrath, F.; Holland, C. Silk Protein Aggregation Kinetics Revealed by Rheo-IR. *Acta Biomater.* **2014**, *10* (2), 776–784. https://doi.org/10.1016/j.actbio.2013.10.032.

(99) Kuo, C. K.; Ma, P. X. Ionically Crosslinked Alginate Hydrogels as Scaffolds for Tissue Engineering: Part 1. Structure, Gelation Rate and Mechanical Properties. *Biomaterials* **2001**, *22* (6), 511–521.

(100) Tse, J. R.; Engler, A. J. Preparation of Hydrogel Substrates with Tunable Mechanical Properties. In *Current Protocols in Cell Biology*; John Wiley & Sons, Inc., 2001. https://doi.org/10.1002/0471143030.cb1016s47.

(101) Jeon, O.; Bouhadir, K. H.; Mansour, J. M.; Alsberg, E. Photocrosslinked Alginate Hydrogels with Tunable Biodegradation Rates and Mechanical Properties. *Biomaterials* **2009**, *30* (14), 2724–2734. https://doi.org/https://doi.org/10.1016/j.biomaterials.2009.01.034.

(102) Anseth, K. S.; Bowman, C. N.; Brannon-Peppas, L. Mechanical Properties of Hydrogels and Their Experimental Determination. *Biomaterials* **1996**, *17* (17), 1647–1657. https://doi.org/https://doi.org/10.1016/0142-9612(96)87644-7.

(103) Chaudhury, S.; Holland, C.; Porter, D.; Vollrath, F.; Carr, A. J. Are They Tought Enough? A Comparison of How The Shear Mechnical Properties of Rotator Cuff Repair Patches Match Normal and Torn Rotator Cuff Tendons. *J. Bone & Jt. Surgery, Br. Vol.* **2012**, *94-B* (SUPP XVIII), 42 LP – 42.

(104) Chaudhury, S.; Holland, C.; Thompson, M. S.; Vollrath, F.; Carr, A. J. Tensile and Shear Mechanical Properties of Rotator Cuff Repair Patches. *J. Shoulder Elb. Surg.* **2018**, *21* (9), 1168–1176. https://doi.org/10.1016/j.jse.2011.08.045.

(105) Chaudhury, S.; Holland, C.; Vollrath, F.; Carr, A. J. Comparing Normal and Torn Rotator Cuff Tendons Using Dynamic Shear Analysis. *J. Bone & Jt. Surgery, Br. Vol.* **2011**, *93-B* (7), 942 LP – 948.

(106) Holland, C.; Vollrath, F.; Gill, H. S. Horses and Cows Might Teach Us about Human Knees. *Naturwissenschaften* **2014**, *101* (4), 351–354. https://doi.org/10.1007/s00114-014-1163-5.

(107) Barnes, J. M.; Przybyla, L.; Weaver, V. M. Tissue Mechanics Regulate Brain Development, Homeostasis and Disease. *J. Cell Sci.* **2017**, *130* (1), 71 LP – 82.

(108) Kurland, N. E.; Dey, T.; Wang, C.; Kundu, S. C.; Yadavalli, V. K. Silk Protein Lithography as a Route to Fabricate Sericin Microarchitectures. *Adv. Mater.* **2014**, *26* (26), 4431–4437. https://doi.org/10.1002/adma.201400777.

(109) Shin, D.-S.; Lee, K.-N.; Jang, K.-H.; Kim, J.-K.; Chung, W.-J.; Kim, Y.-K.; Lee, Y.-S. Protein Patterning by Maskless Photolithography on Hydrophilic Polymer-Grafted Surface. *Biosens. Bioelectron.* **2003**, *19* (5), 485–494. https://doi.org/https://doi.org/10.1016/S0956-5663(03)00228-8.

(110) Hsieh, T. M.; Benjamin Ng, C. W.; Narayanan, K.; Wan, A. C. A.; Ying, J. Y. Three-Dimensional Microstructured Tissue Scaffolds Fabricated by Two-Photon Laser Scanning Photolithography. *Biomaterials* **2010**, *31* (30), 7648–7652. https://doi.org/https://doi.org/10.1016/j.biomaterials.2010.06.029.

(111) Yang, L.-J.; Lin, W.-Z.; Yao, T.-J.; Tai, Y.-C. Photo-Patternable Gelatin as Protection Layers in Low-Temperature Surface Micromachinings. *Sensors Actuators A Phys.* **2003**, *103* (1), 284–290. https://doi.org/https://doi.org/10.1016/S0924-4247(02)00338-2.

(112) Janakiraman, V.; Kienitz, B. L.; Baskaran, H. Lithography Technique for Topographical Micropatterning of Collagen-Glycosaminoglycan Membranes for Tissue Engineering Applications. *J. Med. Device.* **2007**, *1* (3), 233–237. https://doi.org/10.1115/1.2775937.

(113) Liu, W.; Zhou, Z.; Zhang, S.; Shi, Z.; Tabarini, J.; Lee, W.; Zhang, Y.; Gilbert Corder, S. N.; Li, X.; Dong, F.; Cheng, L.; Liu, M.; Kaplan, D. L.; Omenetto, F. G.; Zhang, G.; Mao, Y.; Tao, T. H. Precise Protein Photolithography (P3): High Performance Biopatterning Using Silk Fibroin Light Chain as the Resist. *Adv. Sci.* **2017**, *4* (9), 1700191-n/a.

https://doi.org/10.1002/advs.201700191.

(114) Lee, K.-N.; Shin, D.-S.; Chung, W.-J.; Kim, Y.-K.; Lee, Y.-S. Protein Patterning by Virtual Mask Photolithography Using Micromirror Array. In *2nd Annual International IEEE-EMBS Special Topic Conference on Microtechnologies in Medicine and Biology. Proceedings (Cat. No.02EX578)*; 2002; pp 136–139. https://doi.org/10.1109/MMB.2002.1002280.

(115) Wang, S. D.; Zhang, K. Q. Electrogelation and Rapid Prototyping of Bombyx Mori Silk Fibroin. *Mater. Lett.* **2016**, *169*, 5–9. https://doi.org/10.1016/j.matlet.2016.01.079.

(116) Zhou, Y.; Liang, K.; Zhao, S.; Zhang, C.; Li, J.; Yang, H.; Liu, X.; Yin, X.; Chen, D.; Xu, W.; Xiao, P. Photopolymerized Maleilated Chitosan/Methacrylated Silk Fibroin Micro/Nanocomposite Hydrogels as Potential Scaffolds for Cartilage Tissue Engineering. *Int. J. Biol. Macromol.* **2018**, *108*, 383–390. https://doi.org/10.1016/j.ijbiomac.2017.12.032.

(117) Rnjak-Kovacina, J.; Wray, L. S.; Burke, K. A.; Torregrosa, T.; Golinski, J. M.; Huang, W.; Kaplan, D. L. Lyophilized Silk Sponges: A Versatile Biomaterial Platform for Soft Tissue Engineering. *ACS Biomater. Sci. Eng.* **2015**, *1* (4), 260–270. https://doi.org/10.1021/ab500149p.

(118) Wang, H.-Y.; Zhang, Y.-Q. Effect of Regeneration of Liquid Silk Fibroin on Its Structure and Characterization. *Soft Matter* **2013**, *9* (1), 138–145. https://doi.org/10.1039/C2SM26945G.

(119) Nie, Z.; Kumacheva, E. Patterning Surfaces with Functional Polymers. *Nat Mater* **2008**, *7*

(4), 277–290.

(120) McKendry, R.; Huck, W. T. S.; Weeks, B.; Fiorini, M.; Abell, C.; Rayment, T. Creating Nanoscale Patterns of Dendrimers on Silicon Surfaces with Dip-Pen Nanolithography. *Nano Lett.* **2002**, *2* (7), 713–716. https://doi.org/10.1021/nl020247p.

Dynamic Photo-crosslinking of Native Silk Enables Macro-scale Patterning at Micro-scale Resolution

Anastasia Brif [1,2], Peter Laity [1], Frederik Claeyssens [2] and Chris Holland* [1]*

[1]Department of Materials Science and Engineering Sir Robert Hadfield Building, Mappin Street, University of Sheffield, Sheffield, S1 3JD, UK

[2]Department of Materials Science and Engineering, Kroto Research Institute, Broad Lane, University of Sheffield, Sheffield S3 7HQ, UK

For Table of Contents Use Only